6-11-2015

Morphology and Magnetic Properties of Sulfonated Poly[styrene-(ethylene/butylene)-styrene]/Iron Oxide Composites

Sateesh K. Peddini
Molecular Rebar Design, LLC

Huy N. Pham
University of New Orleans

Leonard Spinu
University of New Orleans, lspinu@uno.edu

James L. Weston

David E. Nikles
The University of Alabama

See next page for additional authors

Morphology and Magnetic Properties of Sulfonated Poly [Styrene-(Ethylene/Butylene)-Styrene]/ Iron Oxide Composites

Sateesh K. Peddini[1], Huy N. Pham, Leonard Spinu[2], James L. Weston, David E. Nikles[3], and Kenneth A. Mauritz[4 *]

[1] *Molecular Rebar Design, LLC, 13477 Fitzhugh Rd, Austin, TX 78736, USA*

[2]*AMRI and Department of Physics, University of New Orleans, LA 70148 USA*

[3]*Center for Materials for Information Technology, University of Alabama, Tuscaloosa, AL, 35487 USA*

[4]*School of Polymers and High Performance Materials, University of Southern Mississippi, Hattiesburg, MS 39406 USA*

Abstract

α-Fe_2O_3 structures were initiated in the sulfonated polystyrene block domains of poly[styrene-(ethylene/butylene)-styrene] (SEBS) block copolymers *via* a domain-targeted *in-situ* chemical precipitation method. The crystal structure of these particles was determined using wide-angle X-ray diffraction and selected area electron diffraction

using a transmission electron microscope (TEM). TEM revealed that for less sulfonated SEBS (10 mole %), nanoparticles were aggregated with aggregate size range of 100-150 nm whereas for high sulfonation (16 and 20 mole % sSEBS) there were needle-like structures with length and width of 200-250 nm and 50 nm, respectively. Dynamic mechanical analyses suggest that initial iron oxide nanoparticle growth takes place in the sulfonated polystyrene block domains. The magnetic properties of these nanocomposites were probed with a superconducting quantum interference device magnetometer at 5 and 150 K as well as with an alternating gradient magnetometer at 300 K. The materials exhibited superparamagnetism at 150 K and 300 K and ferrimagnetism at 5 K.

Keywords: block copolymer templates; iron oxide nanoparticles; magnetic properties

---

*Corresponding Author. Tel.: +1-601-818-1975

E-mail address: kenneth.mauritz@usm.edu (Kenneth A. Mauritz)

Introduction

Styrene based hard/soft block copolymers (BCP) can be used as nanoreactor matrices by rendering the polystyrene (PS) block domains polar through their sulfonation. For example, Mauritz *et al.* [1-4] created metal oxide nanostructures in sulfonated PS domains in hard/soft block copolymers using *in situ* sol-gel chemistry and studied the morphology of the resultant nanocomposites. The main advantage of this assembly process is to have non-aggregated nanostructures with better particle dispersion than that which is affected by conventional mixing methods [5].

Guru *et al.* [6,7] used pre-formed sulfonated (s) poly [(styrene)-(ethylene/butylene)-(styrene)] (sSEBS) films as a growth medium for cobalt ferrite and other metal oxide nanoparticles *via* an *in situ* precipitation method. The synthesized cobalt ferrite nanoparticles were spherical in shape with different sizes at two different reaction times. It was reported that the array of these metal oxide nanoparticles exhibited magnetic properties depending on the temperature.

A macroscopic magnetic material is viewed as an array of small magnetic domains separated by domain walls. Magnetic domains, in turn, are composed of fundamental magnetic moments due to electron spin and orbital contributions, all generally oriented in the same direction throughout the given domain [8-11]. When a macroscopic magnetic material that is ferrimagnetic or ferromagnetic is divided into particles below the size of a critical single domain, domain walls cease to exist. As the particle size further decreases, within the single domain range, a critical threshold is reached, where remanence (M_r) and coercivity (H_c) go to zero (no magnetic hysteresis). When this happens, the system becomes superparamagnetic. For example, the critical single domain size for magnetite and maghemite are 128 and 166 nm, respectively [12].

For iron oxide systems, the critical superparamagnetic size is reported to be approximately below 20 nm [13].

Oxides such as maghemite, cobalt ferrite (generally of the type $MO.Fe_2O_3$, cubic) and barium ferrite ($MO.6Fe_2O_3$, hexagonal) are ferrimagnetic. Bulk maghemite (γ–Fe_2O_3) is ferrimagnetic at room temperature with a saturation magnetization (M_s) and H_c of about 80 emu/g and 250–450 Oe, respectively. Magnetite (Fe_3O_4) is ferrimagnetic with $M_s \approx 92$ emu/g and $H_c \approx 350$ Oe. A polymorph of maghemite is hematite (α–Fe_2O_3), which is of the hexagonal corundum structure and is parasitic or canted antiferromagnetic [14]. Maghemite is only a metastable, low-temperature Fe_2O_3 structure and the phase transition to the α form can take place above 300° C [15]. Detailed analyses of other types of iron oxides and oxyhydroxides such as: η–, ε–, and β– Fe_2O_3 and FeO and FeOOH (its different forms such as α–, β–, γ–, and δ), which have different crystal structures and magnetic properties have been reported [16-32]. This information is provided for the purpose of identifying the synthesized iron oxide nanoparticles with a known macroscopic iron oxide compound.

In principle, the magnetic properties of these nanomaterials can be studied and fine-tuned by manipulating the chemistry of preparation as well as the medium in which they are grown.

Here, we report the preparation and characterization of magnetic nanocomposites created by the precipitation of iron oxide nanoparticles in preformed sulfonated SEBS phase separated templates. The size of the nanoparticles was determined using TEM and their crystal structure was probed using wide angle X–ray diffraction. Inorganic mass uptake was determined using thermogravimetric analysis. Changes in glass transition

temperatures (T_g), as related to morphology, were determined using dynamic mechanical analysis. Magnetic properties were studied using an alternating gradient magnetometer and a superconducting quantum interference device magnetometer.

Experimental

Materials

The commercial SEBS block copolymer, Kraton® G 1652 grade with M_n = 73,600 g mol^{-1} and having ~30% styrene composition, was obtained from Kraton® LLC. The molecular weight of the styrene blocks is 22,150 g mol^{-1} whereas that for the ethylene-butylene block is 51,520 g mol^{-1}. The PDI of the block copolymer is 1.22. Toluene, 1, 2-dichloroethane (DCE), 1-hexanol, acetic anhydride, sulfuric acid, dimethyl acetamide (DMAc), anhydrous ferric chloride ($FeCl_3$), and sodium hydroxide were obtained from Fisher Scientific. All reagents were used without further purification.

Sulfonation reaction

Sulfonation of SEBS was performed according to a procedure reported elsewhere [4, 33]. Here, samples were prepared with three different levels of sulfonation up to 20% by mole. The three sulfonated samples are labeled as follows: 10 mole % sulfonated SEBS = 10SEBS, 16 mole % sulfonated SEBS = 16SEBS, and 20 mole % sulfonated SEBS = 20SEBS. Films of these samples were cast from toluene and hexanol solutions into Teflon® Petri dishes with a thickness of around 1 mm. The films were then dried at 45° C under N_2 for 7d to remove solvents and then annealed at 120° C for 2d under vacuum.

Metal oxide incorporation

Pre-formed films having these sulfonation levels were swollen in DMAc for 48h and constantly shaken. A 3.0 M solution of $FeCl_3$ in DMAc was prepared and the swollen films were submerged in these solutions separately for 48h in a shaker. The samples were taken out and surface wiped with tissue paper to minimize surface precipitation. These iron chloride-doped samples were then washed with DI water several times to leach out excess electrolyte. In the final step, each of the three samples was placed in a freshly prepared 2 M NaOH solution for 48h and washed with DI water continuously for 48h and the water was monitored from time to time to replace the basic water with fresh water to leach out excess Na^+ ions. After washing, samples were dried in an oven for 48h at 120^o C to remove excess solvents and water. A scheme for the sequence of reactions leading to nanoparticle formation is shown in Figure 1 in Supporting Information. In concept, aggregates of hydrated SO_3H groups attached to the styrene blocks provide local polar environments in and around which sorbed ions are energetically compatible. Hence, reactants will be attracted to these regions rather than being homogeneously dispersed throughout a hydrocarbon medium and given high probablilty of reaction as depicted in Figure 1, Supporting Information. Of course, ion exchange reactions involving cations (Na^+, Fe^{3+}) and SO_3H groups must concurrently take place.

Material Characterization

Composite morphology was inspected using transmission electron microscopy (TEM). Samples were cryo-microtomed with a Leica UC FC6. The microtome chamber, sample and knife were maintained at -75^{o} C (beneath the glass transition temperature of the soft ethylene-butylene phase). At least 3 thin sections of ~80 nm were obtained for each sample and placed on a copper grid. Morphology was observed using a JEOL JEM-2100 LaB6 operating at 200 KeV. The particular crystalline nature of nanoparticles was observed with the same microscope in select area electron diffraction (SAED) mode. Crystal structures of metal oxide particles were studied using a Rigaku Ultima III X-Ray diffractometer using a $CuK_{\alpha 1}$ radiation wavelength of 1.54 Å. A continuous scan ranging between 15 and 75^{o} was performed. Jade™ graphical analytical software was used to find the peak positions, relative intensity and full-width-at-half-maximum (FWHM) of the main peak and its 2θ angular position.

Thermogravimetric analysis (TGA) was performed using a TA instruments TGA model Q50. Samples were heated from 30 to 700^{o} C at 10^{o} C/min under nitrogen atmosphere. Dynamic mechanical analysis (DMA) was performed for each metal oxide containing sBCP and its unmodified BCP control to observe the shift of the glass transition temperatures for both the EB and PS (and sPS) block phases before and after metal oxide incorporation. Two trials were performed for each sample to confirm reproducibility of the TGA and DMA experiments, which was indeed the case.

Magnetic measurements of sSEBS/iron oxide samples were performed using a Quantum Design Model MPMS SQUID magnetometer with helium cryostat. Zero field cooled (ZFC) measurements were performed by inserting the sample into the Dewar with the magnetic field set to zero. The temperature was lowered to 5 K and stabilized at this

temperature for 15 min with no applied field. ZFC measurements were then carried out by applying a magnetic field; in this case two different fields (50 and 100 Oe) were applied for each sample separately to study the effect of applied field. Magnetization was measured at this applied field and at each measurement point the system was equilibrated. Measurements were conducted from 5 to 300 K at 5 K increments. For the FC measurements, the system was stabilized at 300 K for 15 min at specified fields (50 and 100 Oe) and measurements were taken at each 5 K decrement until the system reached 5K. Magnetization vs. applied field curves were determined at 5, 150 K for all three samples. The measured magnetization values were divided by the total mass of iron oxide content in sPS block determined from TGA analysis.

Room temperature magnetic measurements were performed using a MicroMag™ Mode alternating gradient magnetometer (AGM, Princeton Measurement Corp.) Films were weighed prior to measurement and mounted on a piezoelectric transducer which oscillates when the sample is subjected to an alternating gradient magnetic field. The alternating field was decreased from 18 kOe to -18 kOe in steps of 100 Oe and increased back to 18 kOe. The magnetization values were divided by the total mass of inorganic oxide content in sPS block, again determined from TGA analysis.

Results and Discussion

Sample analysis

Mole percent sulfonation was determined for each sample prior to film casting using a standard titration method described elsewhere and the values obtained differed from elemental analysis by only 2% [34]. Metal ion incorporation was performed

according to a procedure described elsewhere [35]. DMAc was chosen as a solvent because it selectively swells the sulfonated PS block domains, which promotes the incorporation of metal ions followed by the synthesis of metal oxide particles atom-by-atom in subsequent steps in the sPS block domains.

Figures 1 a, b and c show TGA curves for 10SEBS/iron oxide, 16SEBS/iron oxide and 20SEBS/iron oxide respectively. Inorganic oxide content is expressed as weight percent remaining at 600^{o} C by subtracting the amount of carbon char at the same temperature from that of its unloaded sBCP sample. The iron oxide uptakes were 3.3, 3.6 and 4.6 wt. % respectively for samples in the same order. Iron oxide uptake increases somewhat with increase in percent mole sulfonation in the BCP under the same reaction and *in-situ* precipitation conditions. Moreover, it is seen that these inclusions somewhat increase thermal degradation stability.

Perhaps the greatest shift in TGA decomposition temperatures in moving from 10sSEBS to 10sSEBS/iron oxide composites as compared to moving from 16sSEBS and 20sSEBS to their respective iron oxide composites is related to clustering of SO_3H groups at lower sulfonation levels, as in ionomers. Such clustering, stabilized through electrostatic/hydrogen bonding interactions within, would add to material cohesiveness, thereby enhancing thermal stability, as observed in the TGA curves. On the other hand, beyond 10% sulfonation, as with other ionomers, neat ion clustering breaks down as some ions are distributed, individually or in small multiplets, beyond cluster domains.

Morphology

A wide angle x-ray diffraction (WAXD) pattern for a 10SEBS/iron oxide nanocomposite film is shown in Figure 2. The Miller indices (hkl) for the peaks for this sample listed in Table 1 match those of the α-Fe_2O_3 (hematite) unit cell [36]. The crystal structure of iron oxide is confirmed by using select area diffraction mode in TEM and they are also hematite. Specific peaks for α-Fe_2O_3 are labeled in Figure 1 and the d-spacings and FHTM values were obtained from Jade™ Graphic Analysis software. Approximate particle sizes were calculated from the Scherrer equation [9,37]: $D = (0.9\lambda)/ (FWHM \cos \theta)$, where D = particle size, λ = wavelength of incident x-rays ($CuK_{\alpha 1}$) = 1.54 Å and θ is one-half the diffraction angle 2θ. The Scherrer equation was applied to all the peaks listed in the Table and yielded the same particle size with less than < 5 % deviance. The particle size derived from this equation was 28 nm, which is very close to the range of inter-domain spacing values of the unsulfonated and sulfonated SEBS used in this work and for the styrene-based hard/soft block copolymers found in the literature of Mauritz et al. [3, 4] and Weiss et al. [38].

Figure 3a is a TEM micrograph of a 10SEBS/iron oxide sample. Most of the features appear as clusters of smaller particles that have sizes 100-150 nm, the smallest particle size being ~10 nm. The inset of Figure 3a is an SAED pattern of a single nanoparticle in a cluster which shows short arcs which is the signature of crystals in iron oxide nanoparticle structures. The presence of arcs rather than spots indicates multiple crystals with different orientations relative to the beam. The five main intense arcs correspond to the unit cell structure of α-Fe_2O_3, in harmony with the WAXD results. Figures 3b and c are TEM micrographs of the 16SEBS/iron oxide and 20SEBS/iron oxide composites, respectively. In Figure 3b particle shape is that of bundles of needles with

lengths of 200-250 nm and bundle widths of around 50 nm. In Figure 3c the iron oxide inclusions in the 20 mole % sulfonated SEBS matrix are also composed of similar needle bundles that are 200-225 nm long having widths of around 50 nm. SAED single crystal patterns are observed as insets in both Figures 3b and c. The in-plane lattice dimensions of these single crystal structures were a = 0.4754 and c = 1.299 nm for a hematite unit cell having rhombohedral symmetry [36,39]. The unit cell dimensions obtained from SAED differed from reported values by 6% but, as per earlier literature, this mismatch is considered acceptable for assignment [40].

From these TEM micrographs and SAED crystal patterns it is evident that although the α-Fe_2O_3 nanoparticles grew in elongated sulfonated PS domains they preserved needle-like structures [39] similar to those issuing from large scale conventional precipitation methods. Moreover, the α-Fe_2O_3 structures are observed to exceed the sPS domain sizes of tens of nanometers as discussed below. We speculate that once sulfonated PS block domains are saturated with iron oxide nanostructures, growth continues beyond the confines of these domains to form the observed larger needles.

A general conclusion is that distinct, small crystalline structures, albeit bundled, can in fact be formed within these sulfonated block copolymer templates.

DMA studies were performed on each sample to detect changes in the S and EB block domain glass transitions before and after incorporating the α-Fe_2O_3 nanoparticles. Such results provide indirect evidence regarding assignment of particle location in the sense of chain segmental dynamics modification in a given domain. Figures 4a, b and c show tan δ vs. temperature for the three samples and, for comparison, the results for an

unsulfonated SEBS (0SEBS) control. T_g for both block domains - before and after sulfonation - and then after iron oxide incorporation - are listed in Table 2.

The lowest EB block T_g is that for 0SEBS and this value increases slightly for 10SEBS (+1.3 °C) while the increases for 16SEBS (+3.4 °C) and 20SEBS (+3.8 °C) are somewhat greater. This might be viewed as being due to the formation of strong SO_3H --- SO_3H hydrogen bonding interactions between adjacent chains in the PS domains which add more cohesion within these domains and enhance 'crosslinking' of the rubbery EB chains.

After iron oxide incorporation T_g of the sulfonated block domains increased by 9.9 and 15.9^o C for 16SEBS/iron oxide and 20SEBS/iron oxide, respectively, while the change for 10SEBS was negligible. Given the small T_g changes in the EB block domain, it might be inferred that iron oxide nanoparticles preferentially grow (or at least initiate) in the sPS block domains although there are particles whose dimensions exceed the inter-domain spacings.

The behavior of tan δ at temperatures beyond the PS block phase glass transition shows a high temperature transition in all cases. Blackwell and Mauritz studied the dynamic mechanical properties of these sSEBS triblock copolymers as a function of annealing [4]. Their TEM images for unannealed and unsulfonated SEBS showed well-developed morphology consisting of hexagonal-packed (HP) PS cylinders that were spaced at around 47 nm. 8% sSEBS showed a less ordered phase separated morphology but 14% sSEBS showed distinct lamellar morphology with inter-lamellar spacings of around 30 nm.

In this previous study [4] a high temperature dynamic mechanical transition for unsulfonated SEBS was assigned as an order (HP cylinder order) – disorder (mixed block) transition (ODT) in the usual way. A high temperature transition located at approximately the same temperature for the sulfonated and iron oxide – filled samples was attributed to disruption of SO_3H—rich sub-domains within the PS block domains. It would seem that the high temperature transition for the sSEBS and sSEBS/iron oxide samples in the work presented here is an ODT as modified by electrostatic interactions involving cation-sulfonate groups and α-Fe_2O_3 structures. The ultimate upswing in tan δ for unmodified SEBS might be diagnostic of a 'flow' condition in which the S and EB blocks are mixed. On the other hand, the electrostatic interactions mentioned above would seem to act to hinder flow.

ZFC and FC curves for all three samples were measured at magnetic field strengths of 50 and 100 Oe and are displayed in Figures 5a, b and c. The temperature corresponding to the peak on a ZFC curve gives the blocking temperature (T_B) above which the magnetic moments are thermally randomized. The effect of applied field on T_B was studied by comparing ZFC and FC curves at two different fields. While the ZFC curves exhibit a peak which gives T_B, the width of this peak reflects the distribution of magnetic domain and particle sizes. Below T_B, the material is ferrimagnetic or ferromagnetic i.e., exhibits magnetic hysteresis on applied magnetic field cycling between positive and negative field values. For $T > T_B$, the material exhibits paramagnetism. Nanoparticles that are too small to have domain walls can be superparamagnetic. The convergence of ZFC and FC curves at higher temperatures, and divergence at lower temperatures, is typical for superparamagnetic materials [41]. In

Figure 5 a, the ZFC and FC plots of 10SEBS/iron oxide at 50 and 100 Oe show that T_B at 50 Oe is 50.1 K which is 13.7 K higher than T_B obtained at 100 Oe (36.7 K). From the ZFC and FC curves for 16SEBS/iron oxide and 20SEBS/iron oxide seen in Figures 5 b and c, T_B for 16SEBS/iron oxide decreased by 3 K from T_B = 15 K at 50 Oe to12 K at 100 Oe. For 20SEBS/iron oxide T_B = 16.1 K was the same for both fields.

The ZFC peak width for 10SEBS/iron oxide is wide at both fields indicating a broad distribution of magnetic domains and wide particle size distribution. The SAED pattern of the same sample shown in Figure 3a is in harmony with this wide distribution of particle size, which reflects the mixture of various crystalline ring arcs including rings related to α-Fe_2O_3. The two ZFC curves of the 16SEBS/iron oxide and 20SEBS/iron oxide samples exhibit very narrow and sharp peaks commensurate with very narrow magnetic domain and particle size distributions. The SAED patterns for these samples shown in Figures 3b and c confirm that the matrix-incorporated nanoparticles exist as single crystal structures.

TEM micrographs for the same nanocomposites show nanoparticles with large aspect ratio, and SAED patterns shows there is an existence of single crystals within in these long needle like structures. However, for 10SEBS/iron oxide, the primary particles formed aggregates, which can be understood in terms of a low degree of aggregation of –SO_3H groups. It is speculated that at lower sulfonation levels the iron oxide nanoparticles grow around these reactive ion exchange sites to form 100-150 nm in size aggregated particles.

Magnetization (M) vs. applied magnetic field (H) curves were obtained for samples incorporating the three iron oxide contents at room temperature (300 K) using AGM. A SQUID magnetometer was used for measurements at 5 and 150 K.

Figures 6a and b are M vs. H curves for all three compositions at 5 and 150 K, respectively. At 5 K the coercivities, H_c (magnetic field required to demagnetize) for 10SEBS/iron oxide, 16SEBS/iron oxide, 20SEBS/iron oxide are 497, 292, and 448 Oe respectively. For 16SEBS/iron oxide and 20SEBS/iron oxide, the curves saturate at 80 kOe whereas for 10SEBS/iron oxide there is no saturation at this field strength. The three samples show no hysteresis at 150 K which suggests superparamagnetism because the magnetization and demagnetization curves coincide through the origin. The trend of M_s is that 10SEBS/iron oxide shows the lowest value of 0.4 emu/g, that for 16SEBS/iron oxide is 1.2 emu/g and 20SEBS/iron oxide tends towards saturation at 80 kOe. For 10SEBS/iron oxide and 16SEBS/iron oxide, once magnetization reaches M_s, there is a decrease attributed to the diamagnetic character of the polymer matrix. For samples with higher sulfonation level, i.e. 20 mole %, the iron oxide uptake in the sample is higher and it can be magnetized to saturation under a 80 kOe magnetic field. Whereas, the composites of lower sulfonation levels, 10 and 16 mole %, iron oxide reach magnetic saturation below at 80 kOe due to lower iron oxide intake and the dominating diamagnetic nature of polymer matrix. M vs. H curves for 10SEBS/iron oxide, 16SEBS/iron oxide and 20SEBS/iron oxide samples at 300 K are shown in Figure 6(c). 10SEBS/iron oxide sample exhibits diamagnetism at 300K. This is attributed to the dominating diamagnetic polymer matrix content at lower iron oxide loading levels. The 16SEBS/iron oxide curve saturates at M_s = 2.1 emu/g at an applied field of 18 kOe,

whereas 20SEBS/iron oxide does not saturate at 18 kOe. M_s was obtained by plotting magnetization vs. 1/H and extrapolating the data to zero [9]. M_s thus obtained for 20SEBS/iron oxide is 12.6 emu/g. From M vs. H curves for these three samples at 5 and 150 K, 10SEBS/iron oxide does not saturate at 80 kOe whereas in 16SEBS and 20SEBS there is saturation at 5 K and 150 K. At room temperature, 300 K, iron oxide nanoparticles in the higher sulfonated sample, 20SEBS, do not saturate at 18 kOe whereas the 16SEBS system did. The former might be related to weak surface pinning at the particle surface in the vicinity of $–SO_3H$ groups at 5 and 150 K, whereas at 300 K, interactions between the particle and $–SO_3H$ groups are strong enough to have a stronger surface pinning effect between the particle surface and polymer interface [42, 43]. Surface pinning usually occurs in magnetic nanoparticles dispersed in either fluids or polymer matrices where surface interactions between nanoparticles and the matrix or fluid hinder magnetic moment orientation and/or magnetic domain wall contraction and expansion with an applied external magnetic field. Perhaps surface interactions between iron oxide nanoparticles and $–SO_3H$ groups thermally influence surface pinning effects.

Conclusions

Crystalline iron oxide nanostructures were successfully grown in a sulfonated SEBS block copolymer. These particles initiated from precursor Fe^{+3} and OH^- ions in energetically compatible polar sulfonated PS domains *via in-situ* precipitation. WAXD analysis indicated that the particular crystal structure in 10SEBS/iron oxide was α-Fe_2O_3 with an average particle size of 28 nm which is within the inter-domain spacing values

for SEBS block copolymers which suggests that nanoparticle growth was controlled to an extent by the morphology of the block copolymer.

TEM micrographs showed distinct iron oxide structures in the 10SEBS matrix in the form of clusters of particles ~100-150 nm in size. The formation of nanoparticles can be understood on the basis of aggregation of $–SO_3H$ groups in the less sulfonated samples which present polar environments around which the ionic crystal precursors would be compatible. In 16SEBS and 20SEBS iron oxide structures consist of bundles of distinct needle-like structures with bundle lengths of 200-250 nm and widths of around 50 nm. Selected area electron diffraction patterns for nanoparticles in 10SEBS consisted of narrow arcs that matched with α-Fe_2O_3 (hematite) and in 16SEBS and 20SEBS matrices, iron oxide single crystals were observed with lattice parameters a = 0.4754 nm and c = 1.299 nm with rhombohedral hematite crystal structure with a 6% mismatch with literature values for α-Fe_2O_3. Thermogravimetric analysis determined iron oxide uptakes as 3.3, 3.4 and 4.6 wt. % for 10SEBS, 16SEBS and 20SEBS, respectively.

Dynamic mechanical analyses suggest that the growth of iron oxide nanoparticles initiates mainly in sPS blocks because the T_g of unfilled sSEBS increased with iron oxide incorporation while T_g of the EB phase is less affected. The highest temperature transition, beyond T_g for the hard block phase, is suggested to be an order-disorder transition in SEBS that is modified by the presence of SO_3H groups as well as by the embedded iron oxide particles.

ZFC and FC studies for all three samples determined the blocking temperature for the iron oxide component at two applied fields. M vs. H curves at 5, 150 and 300 K for these three samples showed that the iron oxide nanoparticles exhibited

superparamagnetism at 150 K and 300 K whereas they possessed ferrimagnetism at 5 K with coercivities of 497, 292 and 448 Oe for 10SEBS, 16SEBS and 20SEBS containing iron oxide, respectively.

Acknowledgements

We acknowledge the National Science Foundation Materials Research Science and Engineering Center, Division of Materials Research (DMR-0213883) for Stimuli Responsive Materials at the University of Southern Mississippi for funding. We also thank Kraton® LLC for donating SEBS block copolymers. This work made use of the NSF MRSEC DMR-0213985 Shared Facilities at the University of Alabama for AGM measurements. And for the Work at AMRI/University of New Orleans was supported by DARPA through Grant No. HR0011-07-1-0031.

References

[1] Mauritz KA, Storey RF, Mountz DA, Reuschle DA. Polymer 2002;43(16):4315-4323.

[2] Mauritz KA, Storey RF, Reuschle DA, Beck Tan N. Polymer 2002;43(22):5949-5958.

[3] Mauritz KA, Blackwell RI, Beyer FL. Polymer 2004;45(9):3001-3016.

[4] Blackwell RI, Mauritz KA. Polymer 2004;45(10):3457-3463.

[5] Rajan GS, Sur GS, Mark JE, Schaefer DW, Beaucage G. J Polym Sci Part B Polym Phys 2003;41(16):1897-1901.

[6] Rajan GS, Mauritz KA, Stromeyer SL, Kwee T, Mani P, Weston JL, Nikles DE, Shamsuzzoha M. J Polym Sci Part B Polym Phys 2005;43(12):1475-1485.

[7] Rajan GS, Stromeyer SL, Mauritz KA, Miao G, Mani P, Shamsuzzoha M, Nikles DE, Gupta A. J Magn Magn Mater 2005;299(1):211-218.

[8] Chikazumi S. Physics of Magnetism. New York: John Wiley; 1964.

[9] Cullity BD. Introduction to Magnetic Materials. Addison-Wesley Publishers; 1972.

[10] O'Handley RC. Modern Magnetic Materials: Principles and Applications. 1999.

[11] Spaldin, N. A. Magnetic Materials: Fundamentals and Device Applications. New York:Cambridge University Press; 2003.

[12] Klabunde KJ, Editor. Nanoscale Materials in Chemistry, 2001.

[13] Leslie-Pelecky DL, Rieke RD. Chem Mater 1996;8(8):1770-1783.

[14] Ye X, Lin D, Jiao Z, Zhang L. J Phys D Appl Phys 1998;31(20):2739-2744.

[15] Schimanke G, Martin M. Solid State Ionics 2000;136-137:1235-1240.

[16] Laberty C, Navrotsky A. Geochim Cosmochim Acta 1998;62(17):2905-2913.

[17] Mitov I, Cherkezova-Zheleva Z, Mitrov V. Phys Status Solidi A 1997;161(2):475-482.

[18] Chen L, Yang W-J, Yang C-Z. J Mater Sci 1997;32(13):3571-3575.

[19] Wan M, Fan J. J Polym Sci Part A Polym Chem 1998;36(15):2749-2755.

[20] Sauzedde F, Elaissari A, Pichot C. Colloid Polym Sci 1999;277(9):846-855.

[21] Horak D, Bohacek J, Subrt M. J Polym Sci Part A Polym Chem 2000;38(7):1161-1171.

[22] Rane KS, Verenkar VMS. Bull Mater Sci 2001;24(1):39-45.

[23] Millan A, Palacio F. Appl Organomet Chem 2001;15(5):396-400.

[24] Radhakrishnan S, Saujanya C, Sonar P, Gopalkrishnan IK, Yakhmi JV. Polyhedron 2001;20(11-14):1489-1494.

[25] Wormuth K. J. Colloid Interface Sci 2001;241(2):366-377.

[26] Gonsalves KE, Li H, Santiago P. J Mater Sci 2001;36(10):2461-2471.

[27] Raming TP, Winnubst AJA, van Kats CM, Philipse AP. J Colloid Interface Sci 2002;249(2):346-350.

[28] Chaneac C, Tronc E, Jolivet JP. J Mater Chem 1996;6(12):1905-1911.

[29] Rane KS, Verenkar VMS, Sawant PY. Bull Mater Sci 2001;24(3):331-338.

[30]Venkataraman A, Hiremath VA, Date SK, Kulkarni SD. Bull Mater Sci 2001;24(6):617-621.

[31] Yen FS, Chen WC, Yang JM, Hong CT. Nano Lett 2002;2(3):245-252.

[32] Hiremath VA, Venkataraman A. Bull Mater Sci 2003;26(4):391-396.

[33] Weiss RA, Sen A, Willis CL, Pottick LA. Polymer 1991;32(10):1867-1874.

[34] Blackwell, R. I. Self-Assembled Hybrid Materials Based on Ionomers of Styrene/Ethylene-co-Butylene/Styrene (SEBS): Evolution of Morphology and Rheo-Mechanical Behavior. PhD. Thesis, University of Southern Mississippi, Hattiesburg, MS, May 2004.

[35] Ahmed SR, Kofinas P. Macromolecules 2002;35(9):3338-3341.

[36] Joint Committee on Powder Diffraction Standards, Powder Diffraction File 33–0664 (hematite, α-Fe_2O_3).

[37] Patterson AL. Phys Rev 1939;56:978-982.

[38] Weiss RA, Sen A, Pottick LA, Willis CL. Polymer 1991;32(15):2785-2792.

[39] Minhua C, Tianfu L, Song G, Genban S, Xinglong W, Changwen H, Zhong LW, Angew Chem Int Ed 2005: 44: 4197-4201.

[40] Lee IJ, Kim J-Y, Yu C, Chang C-H, Joo M-K, Lee YP, Hur T-B, Kim H-K. J Vac Sci Technol A 2005;23(5):1450-1455.

[41] Ennas G, Casula MF, Falqui A, Gatteschi D, Marongiu G, Marras S, Piccaluga G, Sangregorio C. J Sol-Gel Sci Technol 2003;26(1/2/3):463-466.

[42] Coey JMD. Phys Rev Lett 1971;27(17):1140-1142.

[43] Linderoth S, Hendriksen PV, Boedker F, Wells S, Davies K, Charles SW, Moerup S. J Appl Phys 1994;75(10, Pt. 2B):6583-6585.

List of Tables

Table 1. Bragg spacings and associated Miller indices for 10SEBS/iron oxide WAXD reflections.

Table 2. Glass transition temperatures for the ethylene-butylene and styrene block domains for unmodified SEBS, sulfonated (s) SEBS and sSEBS containing iron oxide.

List of Figures

Figure 1. (a), (b) and (c): TGA scans of 10SEBS/iron oxide, 16SEBS/iron oxide and 20SEBS/iron oxide, respectively.

Figure 2. WAXD scan for the 10SEBS/iron oxide nanocomposite having 3.3 wt% iron oxide filler. Miller indices of prominent reflections are indicated.

Figure 3. (a), (b) and (c): TEM micrographs of 10SEBS/iron oxide, 16SEBS/iron oxide and 20SEBS/iron oxide samples, respectively. The image insets are SAED diffraction patterns of associated iron oxide crystalline structures. Phase separated morphology of the sSEBS is faintly seen at this magnification.

Figure 4. Tan δ vs. T for (a) 10SEBS/iron oxide, (b) 16SEBS/iron oxide and (c) 20SEBS/iron oxide, respectively.

Figure 5. (a), (b) and (c): ZFC-FC plots of 10SEBS/iron oxide, 16SEBS/iron oxide and 20SEBS/iron oxide measured at 50 and 100 Oe, respectively.

Figure 6. (a), (b) and (c): Overlay M vs. H plots measured at temperatures of 5, 150 and 300 K for 10SEBS/iron oxide, 16SEBS/iron oxide and 20SEBS/iron oxide, respectively.

Table 1. Bragg spacings and associated Miller indices for 10SEBS/iron oxide WAXD reflections.

2θ	d (Å)	(h k l)
23.9	3.712	(0 1 2)
32.9	2.720	(1 0 4)
35.4	2.530	(1 1 0)
39.3	2.291	(0 0 6)
40.7	2.215	(1 1 3)
49.2	1.850	(0 2 4)
53.8	1.702	(1 1 6)
57.1	1.610	(1 2 2)
62.4	1.487	(2 1 4)
63.8	1.456	(3 0 0)

Table 2. Glass transition temperatures for the ethylene-butylene and styrene block domains for unmodified SEBS, sulfonated (s) SEBS and sSEBS containing iron oxide.

Sample ID	T_g of EB block (^oC)	T_g of PS(sPS) block (^oC)
0SEBS	-44.3	94.5
10SEBS	-43.0	97.9
10SEBS/iron oxide	-43.0	96.7
16SEBS	-40.9	102.0
16SEBS/iron oxide	-40.4	111.9
20SEBS	-40.5	105.6
20SEBS/iron oxide	-39.0	121.5

Figure(s)

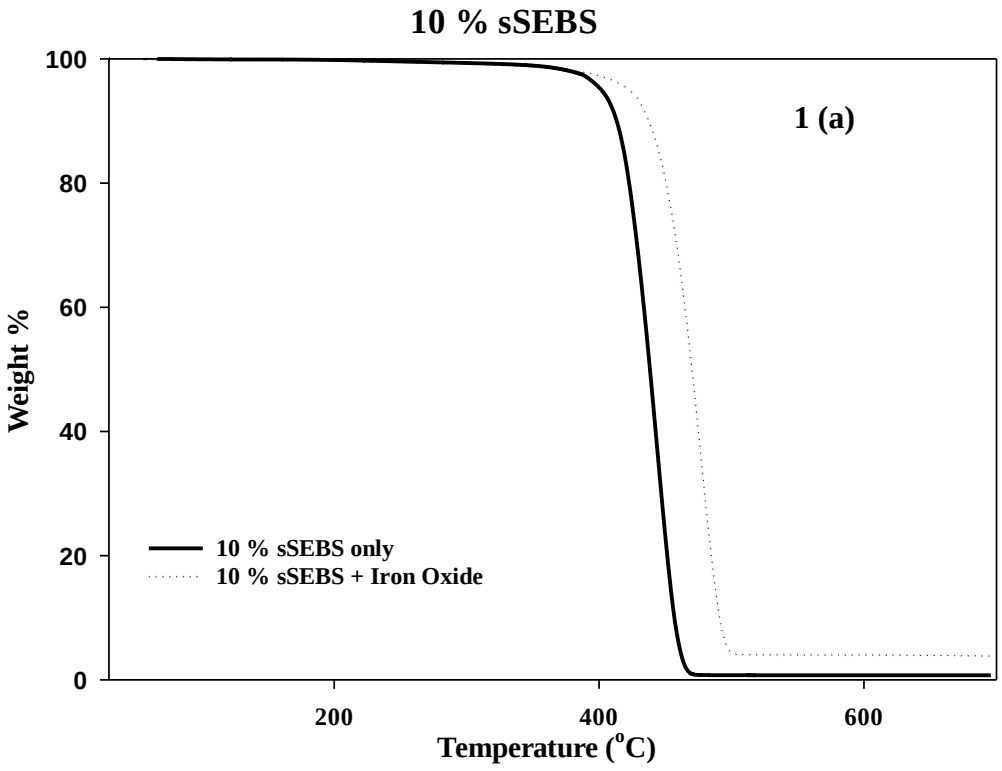
10 % sSEBS
1 (a)
Weight %
100
80
60
40
20
0
200
400
600
Temperature (°C)
10 % sSEBS only
10 % sSEBS + Iron Oxide

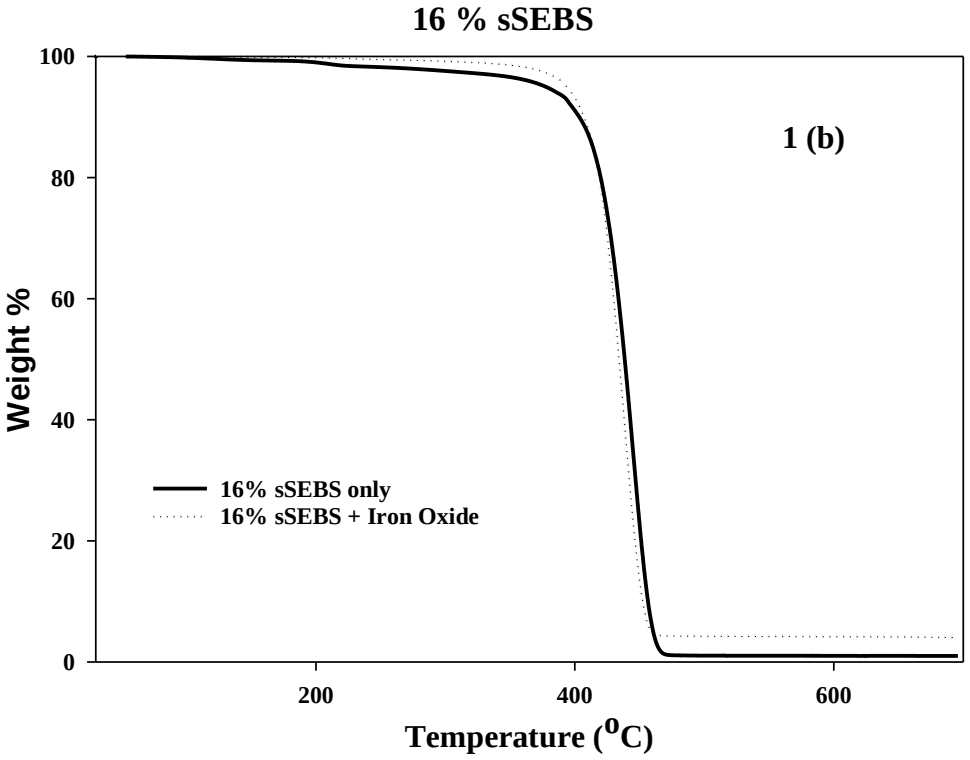
16 % sSEBS
1 (b)
Weight %
100
80
60
40
20
0
200
400
600
Temperature (°C)
16% sSEBS only
16% sSEBS + Iron Oxide

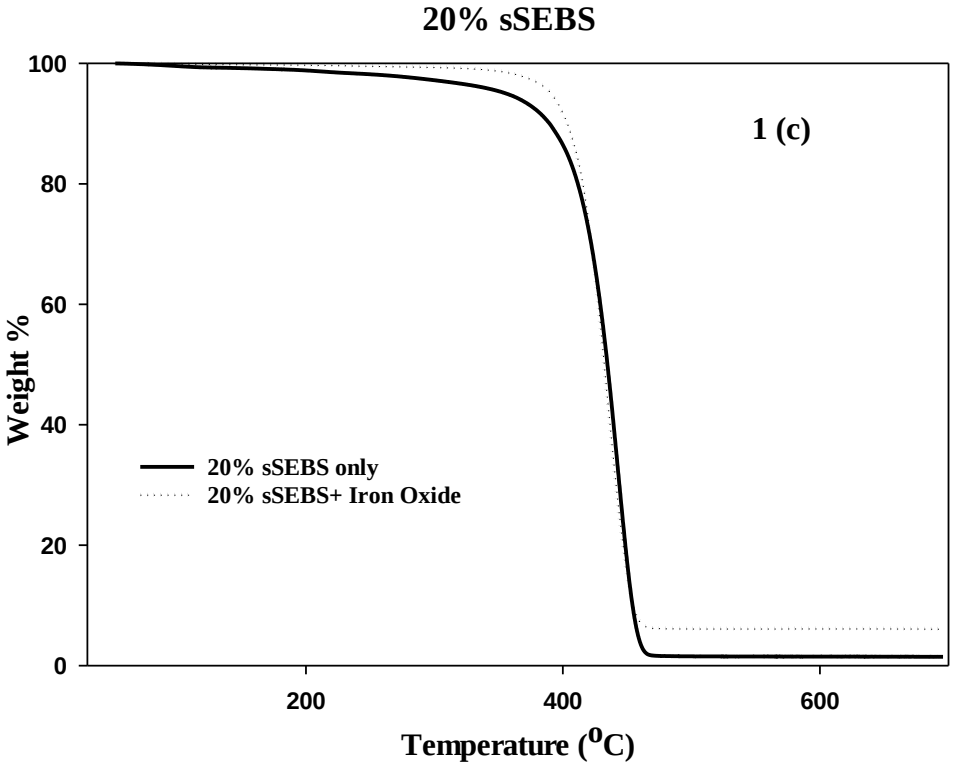

Figure 1. (a), (b) and (c): TGA scans of 10SEBS/iron oxide, 16SEBS/iron oxide and 20SEBS/iron oxide, respectively.

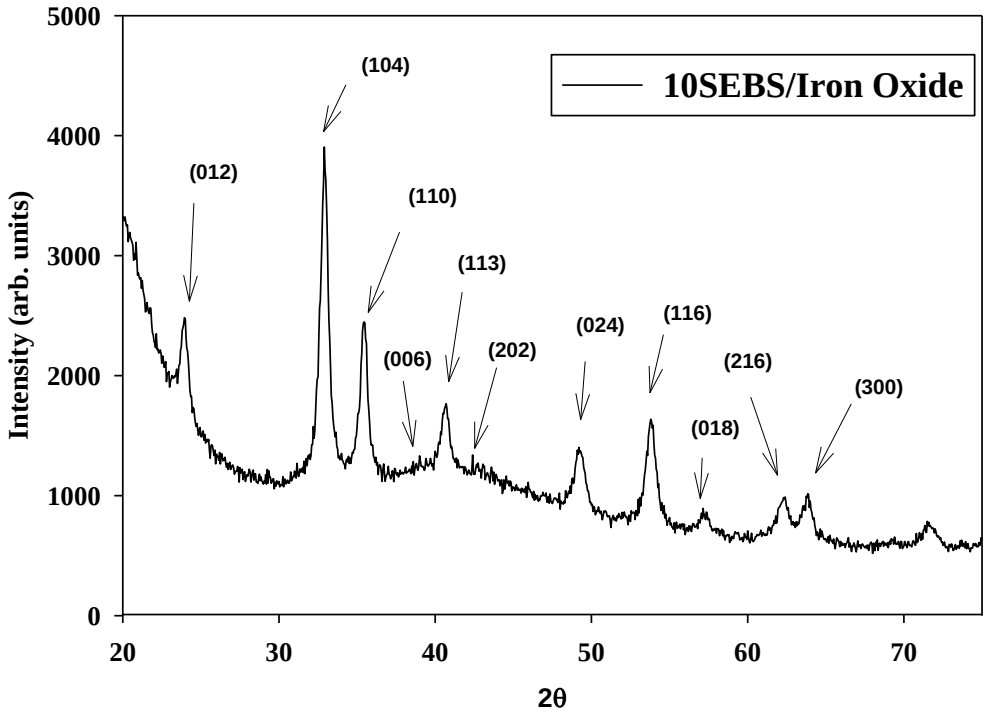

Figure 2. WAXD scan for the 10SEBS/iron oxide nanocomposite having 3.3 wt. % iron oxide filler. Miller indices of prominent reflections are indicated.

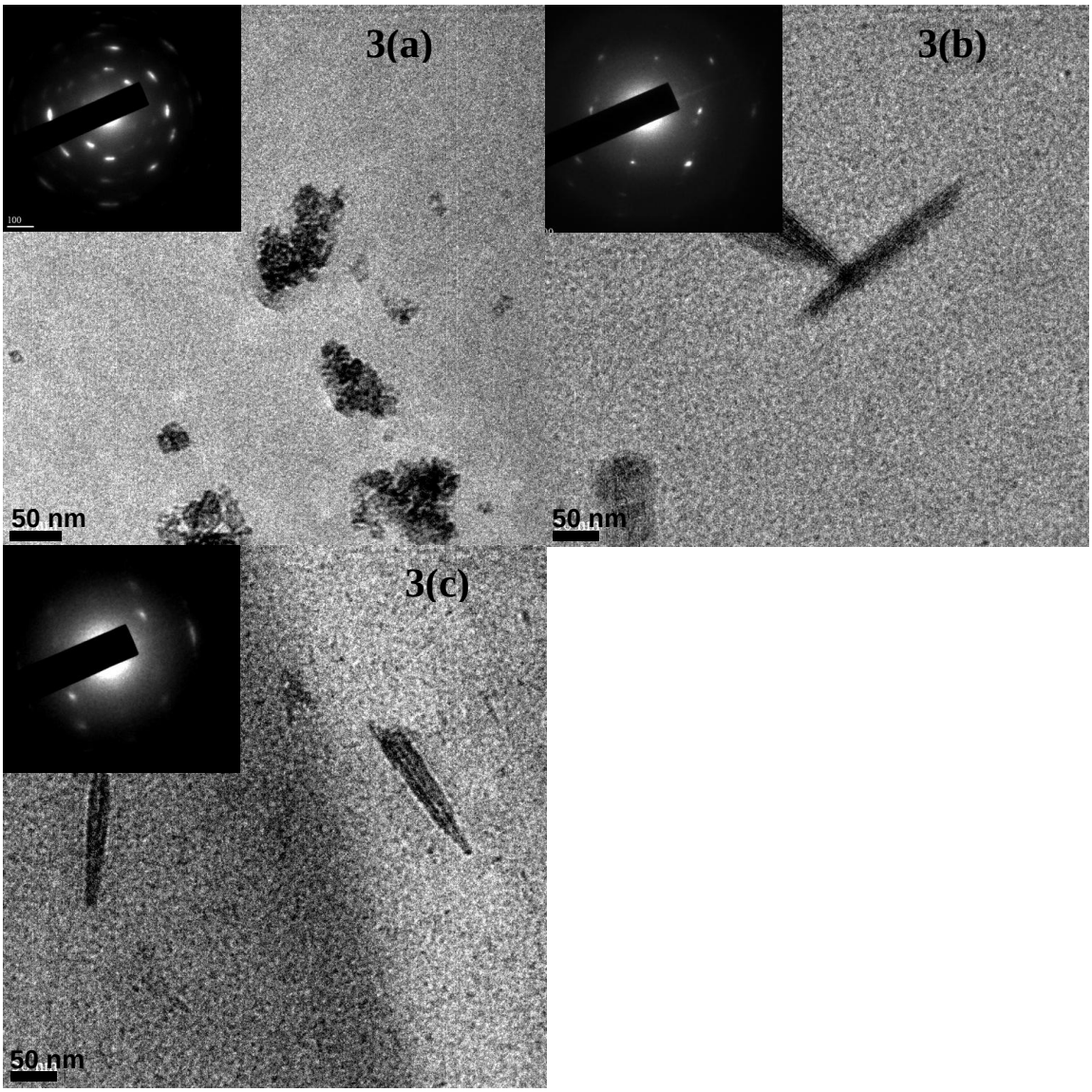

Figure 3. (a), (b) and (c): TEM micrographs of 10SEBS/iron oxide, 16SEBS/iron oxide and 20SEBS/iron oxide samples, respectively. The image insets are SAED diffraction patterns of associated iron oxide crystalline structures. Phase separated morphology of the sSEBS is faintly seen at this magnification (no staining applied).

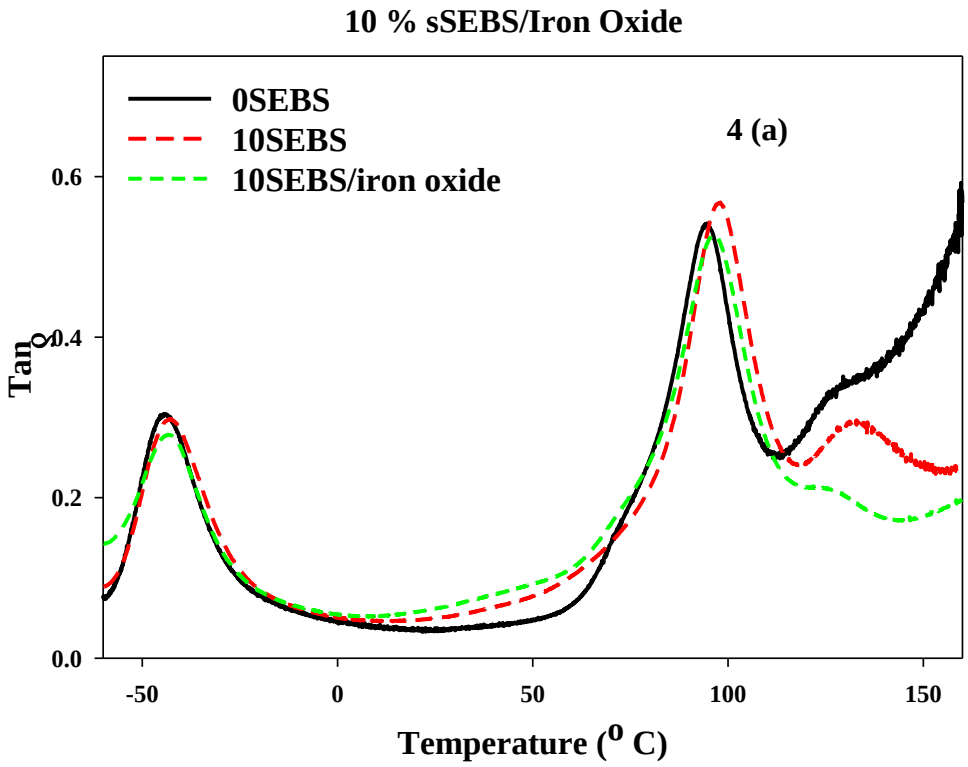
10 % sSEBS/Iron Oxide
0SEBS
10SEBS
10SEBS/iron oxide
4 (a)
Tan δ
0.0
0.2
0.4
0.6
-50
0
50
100
150
Temperature (° C)

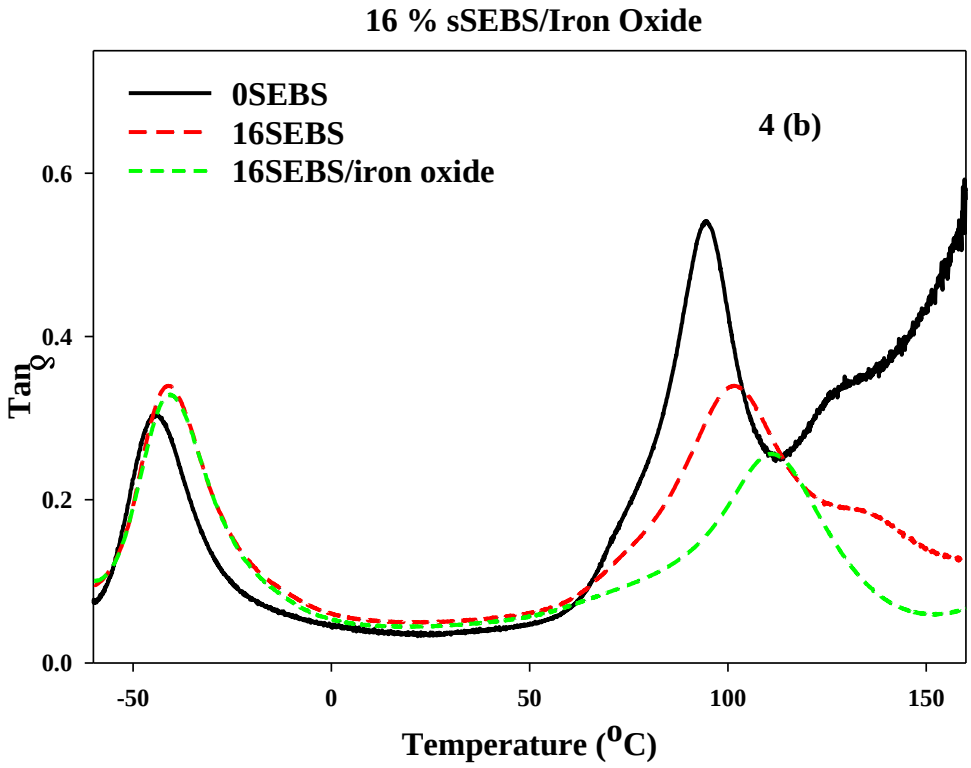
16 % sSEBS/Iron Oxide
0SEBS
16SEBS
16SEBS/iron oxide
4 (b)
Tan δ
0.0
0.2
0.4
0.6
-50
0
50
100
150
Temperature (°C)

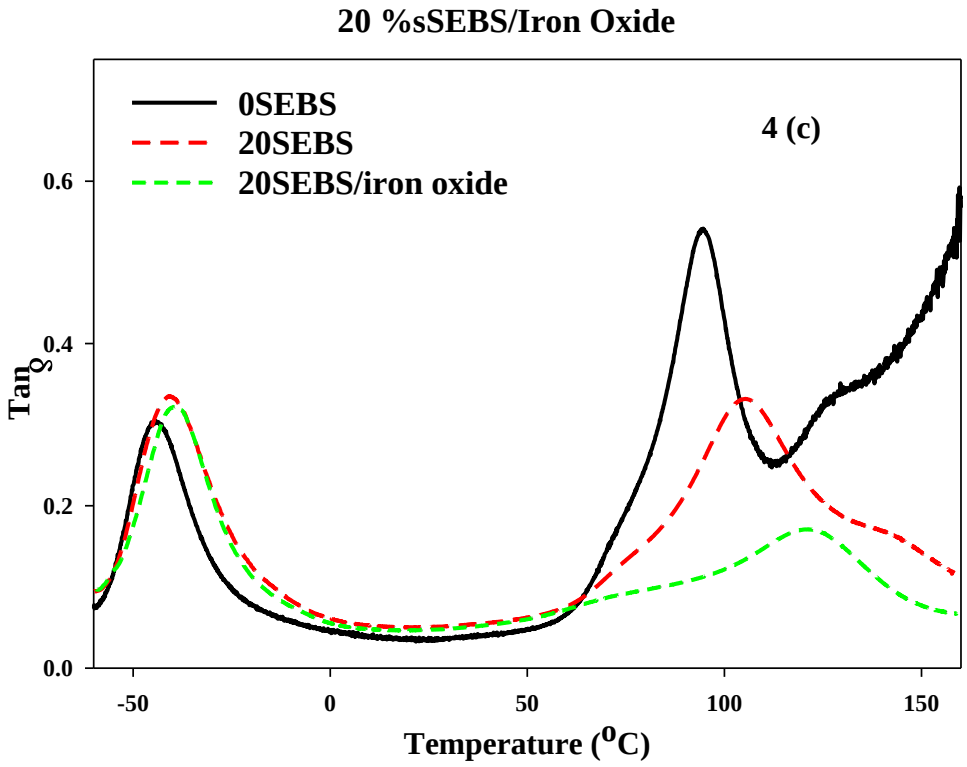

Figure 4. Tan δ vs. T for (a) 10SEBS/iron oxide, (b) 16SEBS/iron oxide and (c) 20SEBS/iron oxide, respectively.

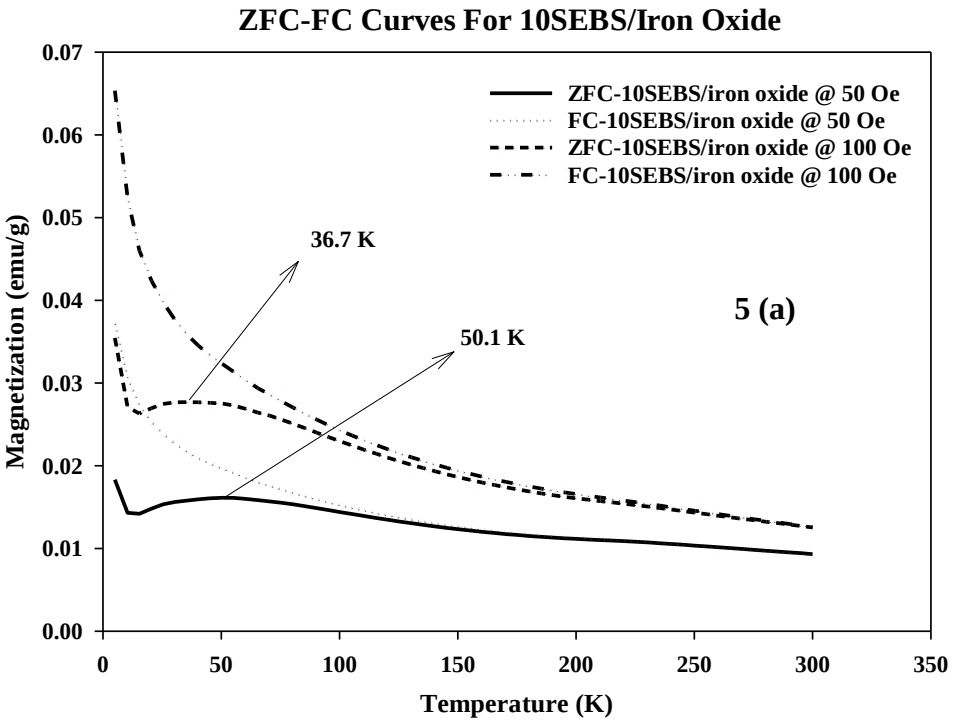
ZFC-FC Curves For 10SEBS/Iron Oxide
ZFC-10SEBS/iron oxide @ 50 Oe
FC-10SEBS/iron oxide @ 50 Oe
ZFC-10SEBS/iron oxide @ 100 Oe
FC-10SEBS/iron oxide @ 100 Oe
36.7 K
50.1 K
5 (a)
Magnetization (emu/g)
Temperature (K)
0.00
0.01
0.02
0.03
0.04
0.05
0.06
0.07
0
50
100
150
200
250
300
350

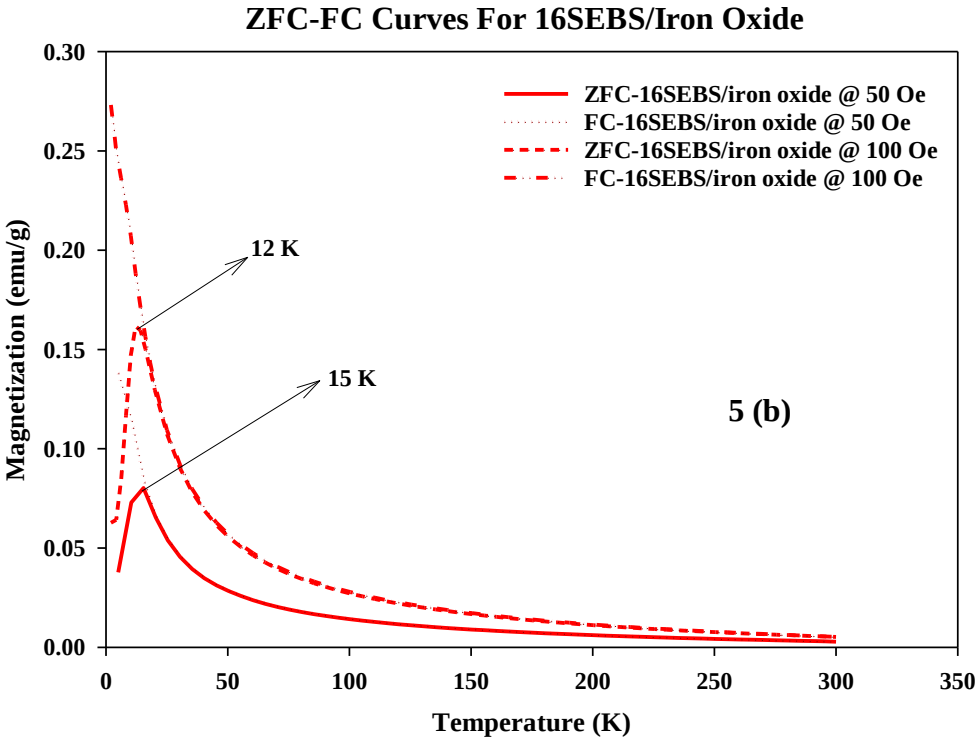
ZFC-FC Curves For 16SEBS/Iron Oxide
ZFC-16SEBS/iron oxide @ 50 Oe
FC-16SEBS/iron oxide @ 50 Oe
ZFC-16SEBS/iron oxide @ 100 Oe
FC-16SEBS/iron oxide @ 100 Oe
12 K
15 K
5 (b)
Magnetization (emu/g)
Temperature (K)
0.00
0.05
0.10
0.15
0.20
0.25
0.30
0
50
100
150
200
250
300
350

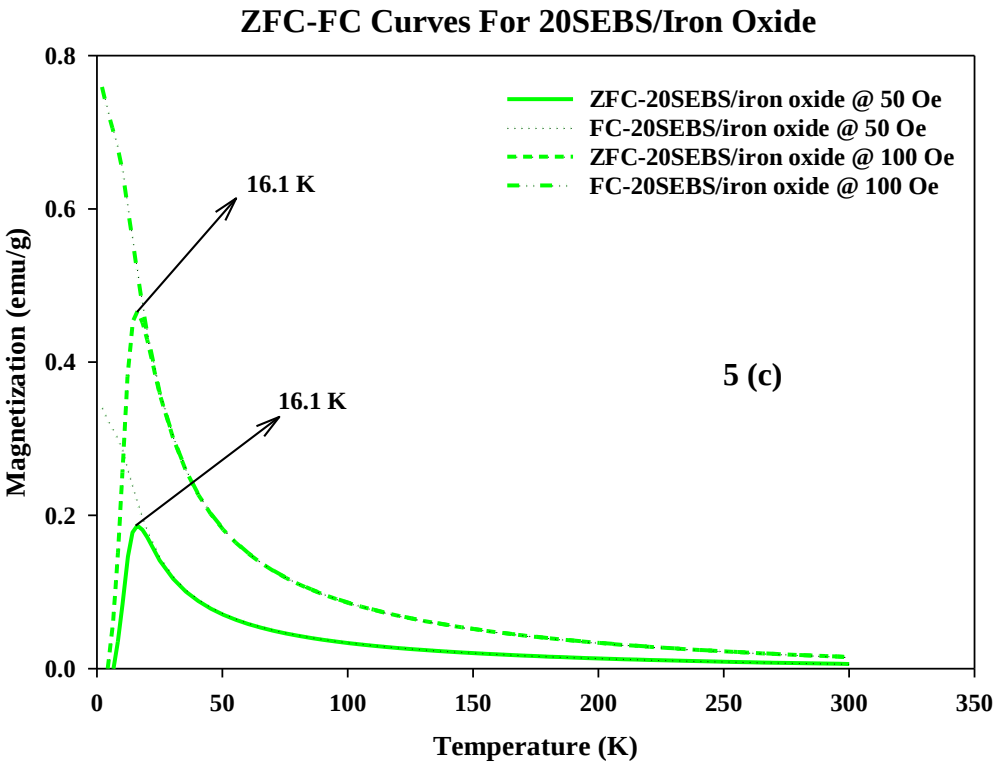

Figure 5. (a), (b) and (c): ZFC-FC plots of 10SEBS/iron oxide, 16SEBS/iron oxide and 20SEBS/iron oxide measured at 50 and 100 Oe, respectively.

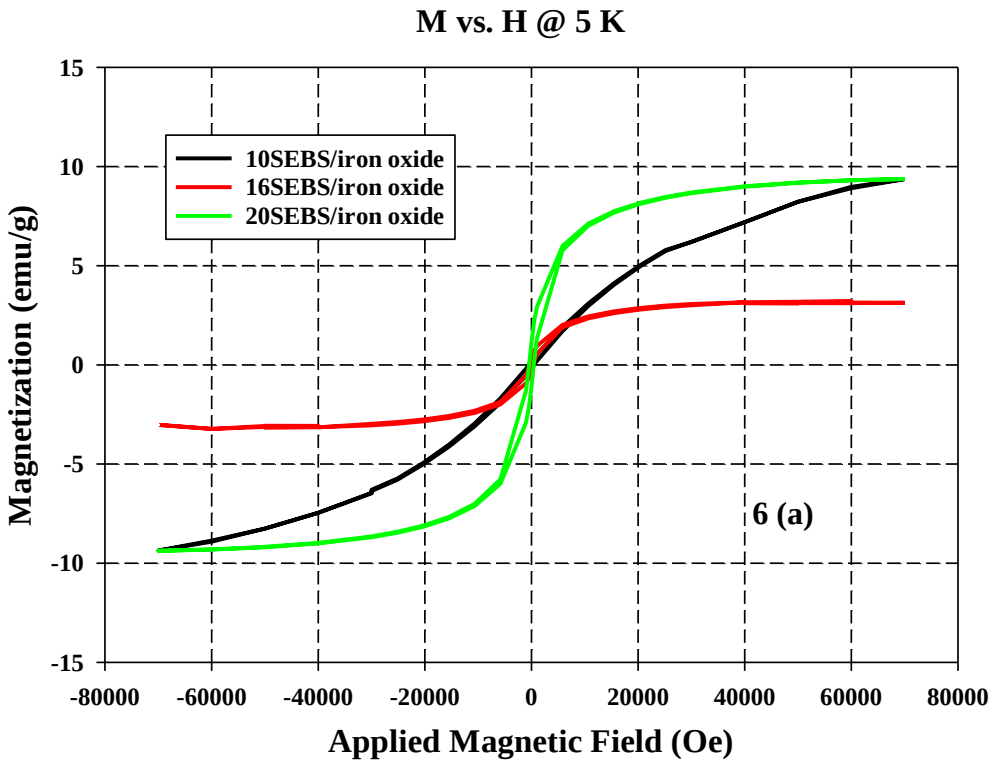
M vs. H @ 5 K
10SEBS/iron oxide
16SEBS/iron oxide
20SEBS/iron oxide
Magnetization (emu/g)
Applied Magnetic Field (Oe)
6 (a)
15
10
5
0
-5
-10
-15
-80000
-60000
-40000
-20000
0
20000
40000
60000
80000

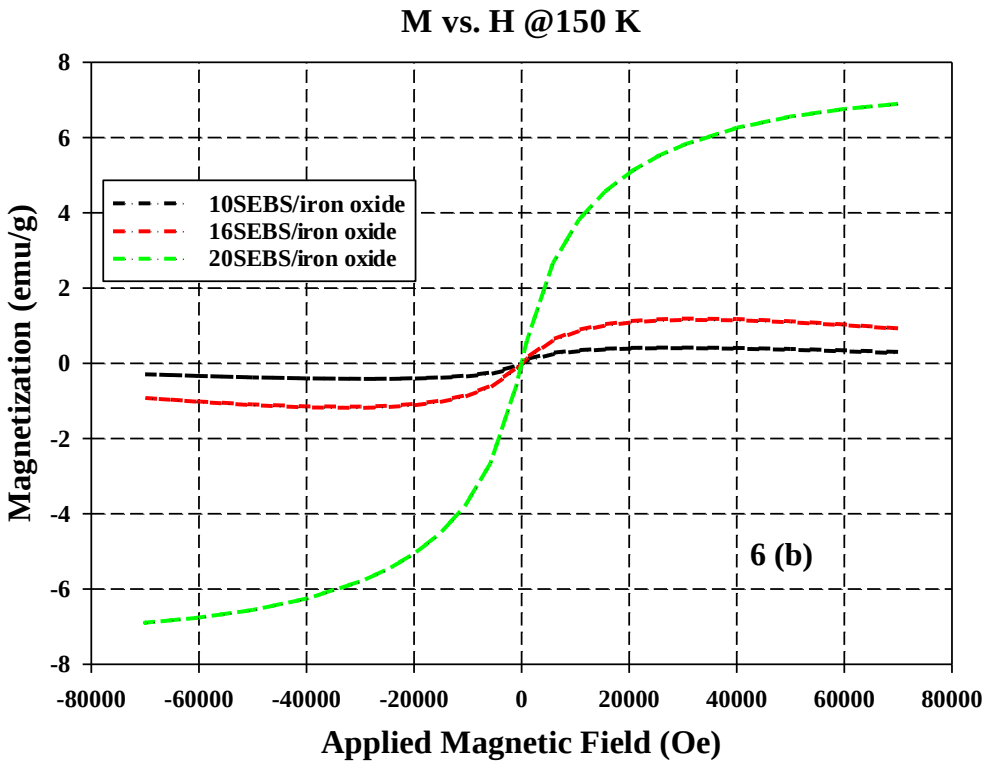
M vs. H @150 K
10SEBS/iron oxide
16SEBS/iron oxide
20SEBS/iron oxide
Magnetization (emu/g)
Applied Magnetic Field (Oe)
6 (b)
8
6
4
2
0
-2
-4
-6
-8
-80000
-60000
-40000
-20000
0
20000
40000
60000
80000

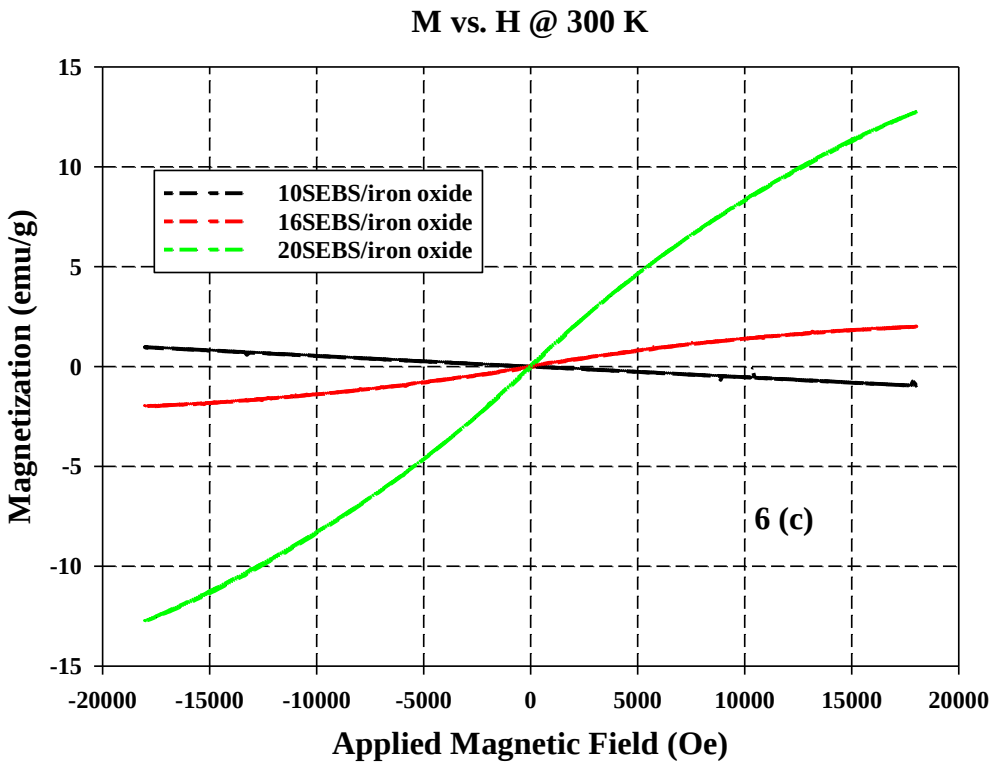

Figure 6. (a), (b) and (c): Overlay M vs. H plots measured at temperatures of 5, 150 and 300 K for 10SEBS/iron oxide, 16SEBS/iron oxide and 20SEBS/iron oxide, respectively.

Graphical Abstract